Brazilian Journal
of Chemical
Engineering

ISSN 0104-6632
Printed in Brazil

Vol. 21, No. 01, pp. 69 - 81, January - March 2004

EXPERIMENTAL STUDY ON BUBBLE SIZE DISTRIBUTIONS IN A DIRECT-CONTACT EVAPORATOR

C. P. Ribeiro Jr. and P. L. C. Lage*

Programa de Engenharia Química, COPPE, Universidade Federal do Rio de Janeiro (UFRJ)
Phone +(55) (21) 2562-8351, Fax +(55) (21) 2562-8300, PO Box 68502,
ZIP Code 21945-970, Rio de Janeiro - RJ, Brazil.
E-mail: paulo@peq.coppe.ufrj.br

(Received: April 15, 2003 ; Accepted: July 2, 2003)

Abstract - Experimental bubble size distributions and bubble mean diameters were obtained by means of a photographic technique for a direct-contact evaporator operating in the quasi-steady-state regime. Four gas superficial velocities and three different spargers were analysed for the air-water system. In order to assure the statistical significance of the determined size distributions, a minimum number of 450 bubbles was analysed for each experimental condition. Some runs were also conducted with an aqueous solution of sucrose to study the solute effect on bubble size distribution. For the lowest gas superficial velocity considered, at which the homogeneous bubbling regime is observed, the size distribution was log-normal and depended on the orifice diameter in the sparger. As the gas superficial velocity was increased, the size distribution progressively acquired a bimodal shape, regardless of the sparger employed. The presence of sucrose in the continuous phase led to coalescence hindrance.
Keywords: bubbles, size distribution, direct-contact evaporation, size measurement, bubble column.

INTRODUCTION

In the so-called direct-contact evaporators a superheated gas is used as the heating fluid for bringing about vaporisation of the solution, into which it is dispersed as bubbles. Due to the absence of any intervening wall separating the processing fluids, these units have many advantages over the traditional shell-and-tube evaporators, among which one can highlight higher thermal efficiency; lower capital, operating and maintenance costs; greater simplicity of construction and the possibility of economically processing highly fouling and/or corrosive solutions. Commercially, this technique has already been utilised for concentrating aqueous solutions of phosphoric acid, sulphuric acid, sodium hydroxide, sodium sulphate and aluminium sulphate (Cronan, 1956).

The superheated gas stream is injected at the bottom of the equipment by means of an adequate distribution system, usually a perforated plate or a set of perforated pipes. During both the formation and ascension of the bubbles through the liquid, there is a natural energy flux from within the bubbles to their surface that produces vaporisation, thereby generating a mass flux from the surface to the inner region of the bubbles.

Since both mass and heat transfer take place at the gas-liquid interface, the available area in a direct-contact evaporator fundamentally depends upon the bubble size distribution and may therefore vary with operating conditions. Although some models for estimating the size of the bubble formed at the sparger have already been proposed (Mezavilla, 1995; Campos and Lage, 2000), these estimates might not be valid for all of the equipment on

*To whom correspondence should be addressed

account of the breakage and coalescence phenomena which result from bubble interactions during the ascension stage.

For isothermal bubbling, many studies on bubble size distributions can be found in the literature (Kölbel et al., 1961; Todtenhaupt, 1971; Hebrard et al., 1996; Camarasa et al., 1999; Colella et al., 1999; Polli et al., 2002; Schäfer et al., 2002). Nonetheless, Silva and Lage (2000) seem to be the only ones to have reported results related to non-isothermal bubbling. The number of bubbles analysed by these authors, though, was less than 200, which statistically is not enough to characterise the shape of the distribution. In all these studies, only the homogeneous bubbling regime was considered.

Therefore, in this work, a photographic methodology was employed to measure statistically significant bubble size distributions under different operating conditions in a direct-contact evaporator, including both the homogeneous and the heterogeneous bubbling regime.

MATERIALS AND METHODS

Experimental Set-up

The experimental set-up used for conducting the evaporation experiments is represented in Figure 1. The system is fed with dry compressed air (dew point at 0^oC). Initially, the air is sent to one of the three rotameters available for measuring the feed flow rate, which has an error estimated at about 5%. In all runs, the gauge pressure in the air line was kept equal to 4×10^5 Pa.

Once the flow rate is determined, the air is taken to the heating system, which consists of an electric oven whose maximum power equals 2000 W. Within the oven, the air flows in an AISI 316 stainless steel serpentine 6.35 mm in nominal diameter with a length of about 23 m. A type K thermocouple registers the operating temperature of the oven, whose value is always kept below the working limit for AISI 316 stainless steel (650^oC) by means of a system of on-off control of the voltage applied to the electrical resistances.

The pipe inside which the heated air flows from the oven outlet to the bottom of the column is thoroughly isolated with ceramic fibre. Aiming at minimising the energy loss from the gas to the surroundings, an electrical resistance with an overall power equal to 160 W was coiled around this part of the pipeline.

The gas temperature is measured both at the oven outlet and in the chamber beneath the sparger using type K thermocouples, whose sensors are located in the middle of the cross section of the pipes with the aid of tee fittings. After the first thermocouple there is a needle valve for controlling the airflow rate in the by-pass line used during the transient heating of the oven, as explained in the next section. Beyond this valve there is another needle valve which controls the rate of gas flow fed into the equipment.

The evaporator consists of a glass column 7.3 cm in inner diameter and 70 cm in height, at the bottom of which the sparger is placed and whose top is closed with an aluminium lid sealed with Viton® O-rings. A platinum resistance thermometer (PT-100), 1.0 m in length, is placed in this lid for measuring the liquid temperature.

The gas distribution system is composed of two sintered AISI 316 stainless steel plates 3.24 and 2.19 mm in thickness, both with a diameter of 8.0 cm. Different regions of the surface of the thinner plate, which is in contact with the liquid during operation, were analysed in a scanning electron microscope and a mean pore diameter of (12 ± 5) μm was determined for this plate. On top of this porous plate two different perforated plates may be used, one made of copper and another made of AISI 316 stainless steel, both of them 0.53 mm in thickness and 8.0 cm in diameter, containing 89 orifices with a diameter of 0.5 mm arranged in a quadrangular pattern with a pitch of 6.3 mm. The desired set of plates is fixed between two flanged aluminium pieces, with the glass column fitted into the upper aluminium piece, in which there is an outlet pipe for liquid removal. The system is sealed with Viton® O-rings and graphoil. The bottom of the column rests on insulating bricks, which are covered with ceramic fibre to increase the efficiency of the thermal insulation.

The lateral area of the evaporator is insulated with a glass fibre piece for pipe insulation, which is divided into two equal parts. One half is fixed to the column wall and a graduated scale is glued onto it for measuring the overall height of the mixture in the column. The other half, attached to the first one, can be moved by rotation for photographing the two-phase mixture and reading its overall height. All photos were taken with a SONY digital camera (model MAVICA® MVC-FD91), adjusting the shutter speed setting so that the required illumination was provided by the flash of the camera itself.

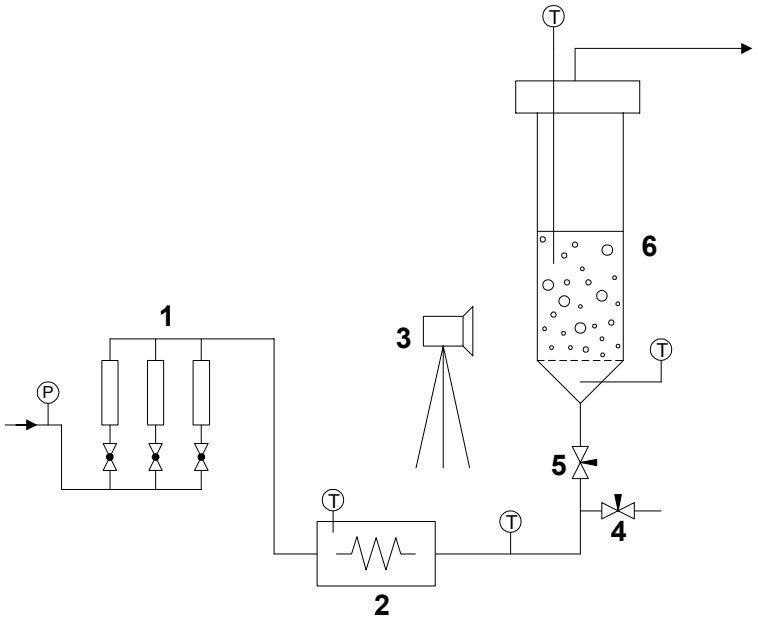

Figure 1: Experimental set-up for evaporation tests: 1 - rotameters; 2 - electrical oven; 3 - camera; 4 - by-pass valve; 5 - main valve; 6 - evaporator.

Experimental Procedure

At the beginning of each run, the evaporator feeding valve was closed and the by-pass valve was opened to the desired airflow rate. The electrical oven was turned on and while it was reaching its steady-state temperature, the photographic camera was appropriately positioned. When the operating temperature had been reached, a previously weighed mass of liquid was poured into the column, the liquid height without bubbling was recorded and then the heating resistance of the pipe between the oven and the evaporator was turned on. The by-pass valve was closed and the evaporator valve was immediately opened to the desired airflow rate, so that bubbling commenced. The overall mixture height was read and the glass fibre insulation was closed.

Aiming at determining the bubble size distribution, five pictures of the two-phase mixture in the region close to the sparger (about 0.11 m above it) were periodically taken. Apart from that, periodical readings of the air temperature at the oven outlet and at the column inlet, the liquid temperature and the overall mixture height were made. Each experiment was conducted up to the point when quasi-steady-state regime had been reached, after which the liquid temperature does not vary with time.

In the photos taken in the quasi-steady-state regime, the area of the bubbles was determined based upon the graduated scale fixed to the side of the column. This scale was located in the centre plane of the column, on which the camera was focussed for all experiments. All photos were analysed using the software Tnimage, version 3.2.0 (Nelson, 2000), which enables quantification of the number of pixels associated with any area delimited in a picture. Thus, in each photo, different regions with the same area were selected in the image of the graduated scale, so as to obtain a relationship between the areas in pixels and in square millimetres. Next, the contours of the bubbles on focus were manually traced, the area of each of them determined and then the diameter of the circle with the same area computed. Based on a hypothesis of random positioning of the bubble in the photographic plane, this diameter was considered to be equivalent to the one related to the sphere with the same volume. A minimum of 450 bubbles was analysed for each experimental condition in order to guarantee the statistical significance of the determined size distributions (Colella et al., 1999).

Due to the curved surface of the glass column and to the considerable differences between the refractive indices of glass and air, there is a systematic parallax error in the measurement of the bubble areas by the photographic technique. In order to quantify this error, the previously described procedure was utilised to determine the diameter of a steel sphere similar in size to the bubbles. The pictures were taken with the sphere placed in three different positions: at the centre of the column, halfway between the centre and the wall of the column and near the wall. With the aid of a

micrometer, the real diameter of the steel sphere was measured (d = 4.77 ± 0.01 mm), thereby defining a correction factor for the parallax effect equal to the ratio of the real area of the cross-section of the sphere to the mean value obtained by the photographic technique. For the sphere placed at the centre of the column, the correction factor was (0.68 ± 0.02), whereas, halfway between the centre and the wall of the column and near the wall, the values obtained were both equal to (0.71 ± 0.03). Since these intervals overlap, a single correction factor, equal to the mean of these individual values (0.69 ± 0.03), was adopted for all positions within the column. It should be emphasised that the validity of this photographic technique had been previously confirmed by Silva and Lage (2000).

RESULTS AND DISCUSSION

Effect of the Gas Flow Rate

Initially, using the stainless steel perforated plate as sparger and keeping the initial mass of liquid in the column at a constant value, the effect of the gas flow rate was studied. Experiments in duplicate and in a random order were carried out for four different gas superficial velocities, calculated assuming the gas to be at the liquid quasi-state-state temperature (340 K), whose values are listed in Table 1. Examples of the photos of the two-phase mixture taken in the quasi-steady-state regime for the minimum and maximum gas flow rates are shown in Figure 2.

Table 1: Mean bubble diameters (experiments in duplicate) for the stainless steel perforated plate and different gas superficial velocities.

U_G (cm/s)	d_{10} (mm)	d_{30} (mm)	d_{32} (mm)
2.2 ± 0.1	4.5 ± 0.1	4.9 ± 0.1	5.3 ± 0.8
	4.4 ± 0.1	4.7 ± 0.1	5.1 ± 0.7
4.4 ± 0.2	5.7 ± 0.2	6.4 ± 0.2	7 ± 1
	5.4 ± 0.2	6.4 ± 0.2	8 ± 1
6.6 ± 0.3	6.6 ± 0.2	7.9 ± 0.2	10 ± 1
	6.5 ± 0.2	8.3 ± 0.3	11 ± 2
12.1 ± 0.6	8.0 ± 0.2	9.5 ± 0.3	11 ± 2
	8.5 ± 0.3	10.7 ± 0.3	13 ± 2

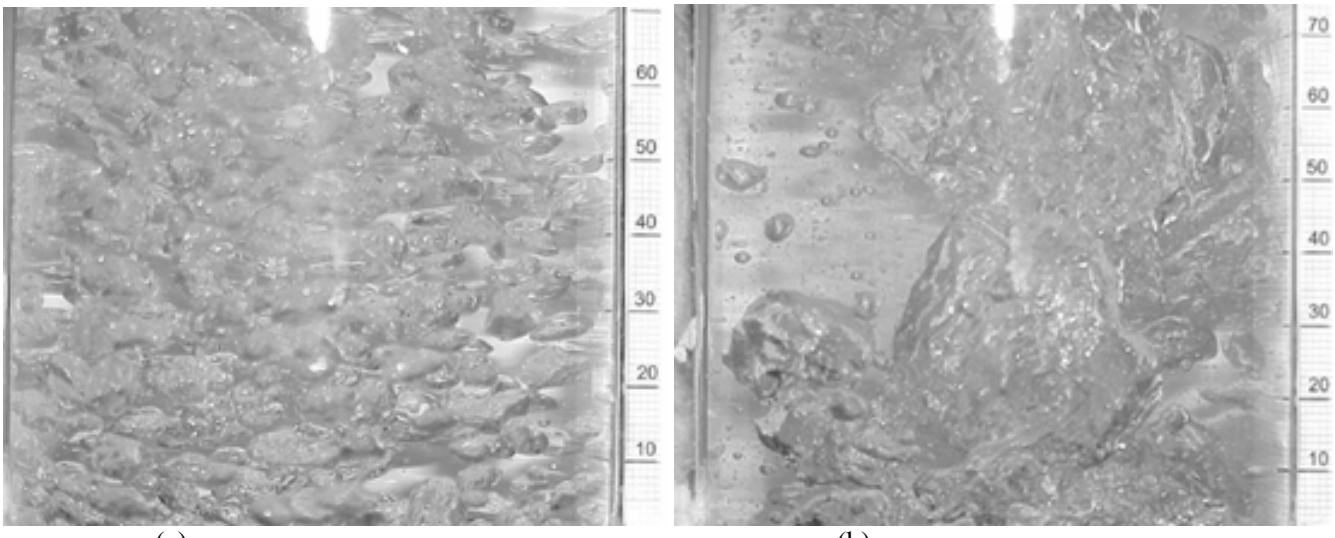

(a) (b)

Figure 2: Photos of the two-phase mixture: (a) U_G = 2.2 cm/s and (b) U_G = 12.1 cm/s.

The changes in the bubbling configuration are easily observed. For U_G = 2.2 cm/s, there is little variation in the size of the bubbles and these are evenly distributed in the radial position, characterising the homogeneous bubbling regime (Ruzicka et al., 2001). In contrast, when U_G = 12.1 cm/s, a wide variation in the size of the bubbles is observed. Besides, a radial gradient in the concentration of bubbles and, accordingly, in the gas hold-up is evident. These two characteristics point to the heterogeneous bubbling regime.

Photos such as the ones exemplified in Figure 2 were utilised in the determination of the bubble size distributions. Nineteen classes in the range $0 < d \leq 34$ mm were considered. For each flow rate, the pictures related to the two runs were independently analysed, resulting in a duplicate for each size distribution, as portrayed in Figure 3. The error bars shown in the aforementioned picture were calculated using the equations given below, developed as explained in the appendix by applying the error theory to the definition of the relative frequency for each class, H_i:

$$\Delta H_i^+ = \frac{1}{NB}\sum_{k=1}^{NB}\left[\int_{d_k}^{d_k+\Delta d_k}\delta(d_k - h_i)\,d(d_k) + \int_{d_k-\Delta d_k}^{d_k}\delta(d_k - h_{i+1})\,d(d_k)\right] \quad (1)$$

$$\Delta H_i^- = \frac{1}{NB}\sum_{k=1}^{NB}\left[\int_{d_k-\Delta d_k}^{d_k}\delta(d_k - h_i)\,d(d_k) + \int_{d_k}^{d_k+\Delta d_k}\delta(d_k - h_{i+1})\,d(d_k)\right] \quad (2)$$

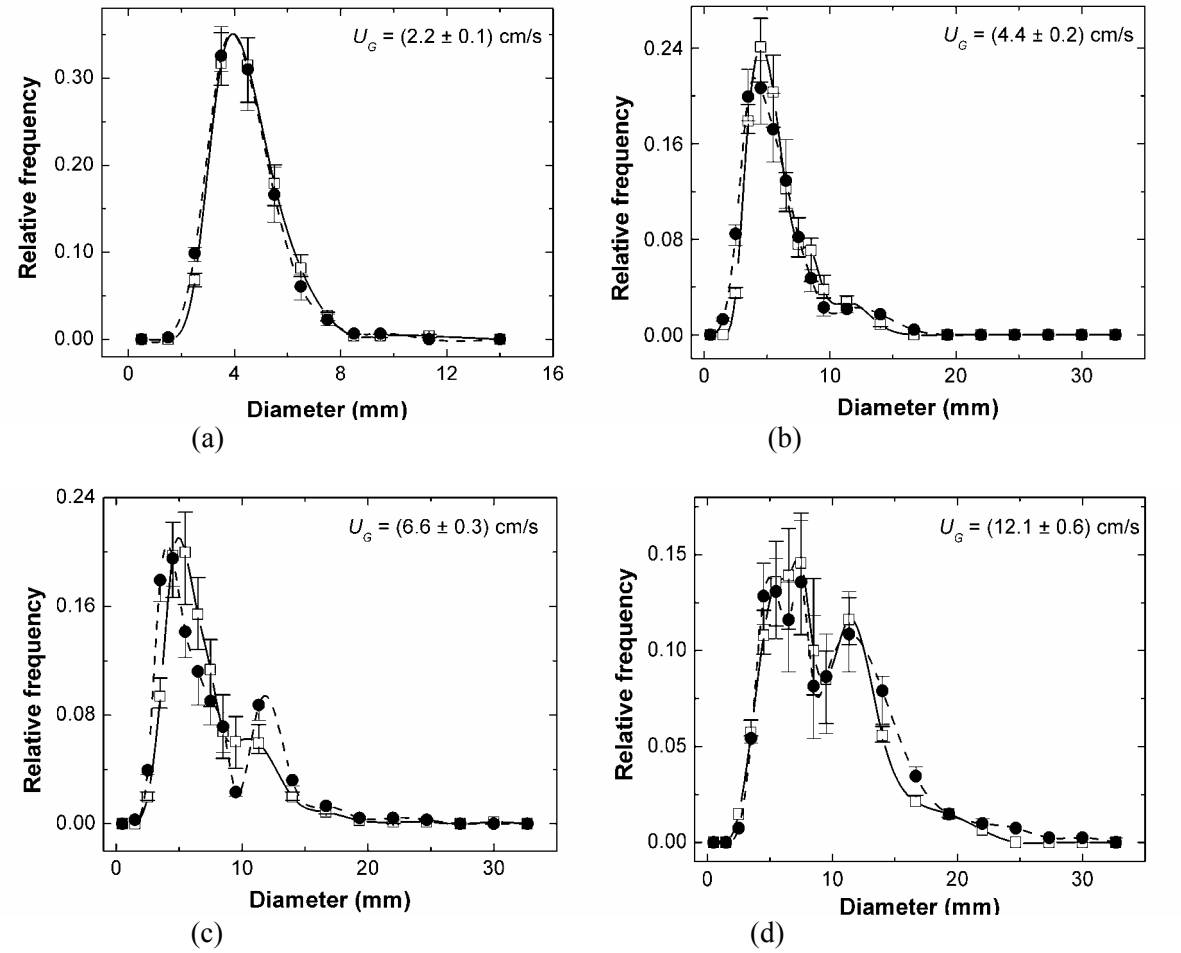

Figure 3: Bubble size distributions in duplicate for four different gas superficial velocities.

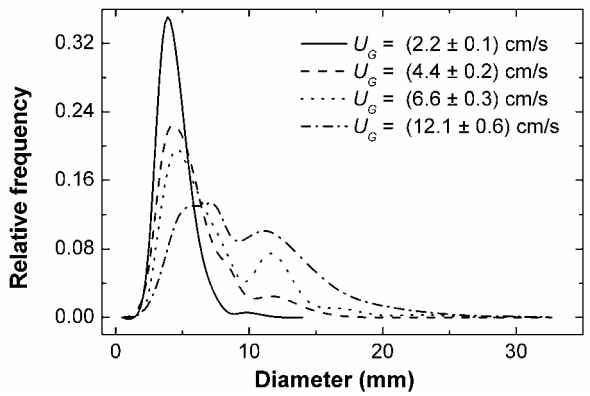

Figure 4: Effect of gas superficial velocity upon bubble size distributions.

With the lowest superficial velocity, the two measured distributions practically coincide with each other. As U_G increases, the scatter between the two data sets seems to increase, though this scatter is well represented by the error bars, since an intersection between the ranges of relative frequency is verified for most classes. These results not only represent strong evidence of the reproducibility of the bubble size distribution data determined in this work, but also suggest that the error estimate for the relative frequency of each class is adequate.

In view of the fact that the two curves for each U_G value in Figure 3 in fact represent different estimates of the same quantity, these curves were used to calculate the mean bubble size distribution associated with each gas superficial velocity. The comparison between these mean values is presented in Figure 4. The unimodal shape of the distribution related to the lowest superficial velocity, with a reduced size range and a high fraction of smaller bubbles, is typical of the homogeneous bubbling regime and agrees with data available in the literature for isothermal bubbling with the air-water system (Hebrard et al., 1996; Polli et al., 2002). As a result of the increase in gas superficial velocity, the distribution widens, including sizes which were previously unobserved. Moreover, the fraction of small bubbles decreases and the initial peak is progressively shifted towards the region of higher diameters. With the increasing number of large bubbles a second peak in the distribution appears, already visible for U_G = 6.6 cm/s. This bimodal feature of the bubble size distribution in the heterogeneous regime is in agreement with the results of gas disengagement experiments reported for isothermal bubbling (Vermeer and Krishna, 1981; Ellenberger and Krishna, 1994). Even though the bubble formation diameter in the orifices of the sparger increases with gas superficial velocity, this particular effect does not justify, for instance, the appearance of a second peak in the distributions. Actually, the observed changes derive fundamentally from coalescence, which like breakage increases in frequency as gas superficial velocity increases (Prince and Blanch, 1990; Millies and Mewes, 1999).

With the size distribution data one may compute any mean bubble diameter using the general equation below:

$$\left(d_{pq}\right)^{p-q} = \frac{\int_0^\infty d^p F(d)\ d(d)}{\int_0^\infty d^q F(d)\ d(d)} \cong \frac{\sum_{i=1}^{NC} d_i^p H_i}{\sum_{i=1}^{NC} d_i^q H_i} \qquad (3)$$

Specifically, in this work, three mean bubble diameters were calculated, namely, the numeric mean diameter, d_{10}, the volumetric mean diameter, d_{30}, and the Sauter mean diameter, d_{32}, which represents the ratio of the total gas volume to the interfacial area in the two-phase mixture. The results obtained are listed in Table 1. All deviations presented in this table were computed applying the error theory to Eq. (3).

It can be verified in the aforementioned table that, regardless of its definition, the mean bubble diameter increases with U_G, a fact that had already been evidenced by the data in Figure 4. In this case, it is interesting to compare the information contained in each definition of d. Even though the deviation associated with d_{32} is high and sometimes does not allow one to differentiate this mean diameter from the other two, the data in Table 1 follow the pattern $d_{10} < d_{30} < d_{32}$, a tendency that becomes clearer as U_G increases. As the arithmetic average, d_{10} focuses only

on relative frequency and, hence, is scarcely affected by the bigger bubbles that are present in a reduced number, an inconvenience observed to a lesser extent for both d_{30} and d_{32}, since the former includes the effect of diameter on volume and the latter takes into account the influence of diameter on both volume and area. Therefore, the value of d_{10} is only suitable for characterising the bubble size distribution in the homogeneous bubbling regime.

A simplification frequently adopted in the modelling of bubble columns operating in the heterogeneous regime is to consider two mean bubble diameters: one related to the "small" bubbles, generated by the sparger, and another associated with the "large" bubbles produced by coalescence. With the aim of determining a characteristic size for these two kinds of bubbles, the size distributions were divided into two regions according to the limits of the peaks, in view of the fact that the appearance of the second peak in the distribution is precisely due to coalescence. The proposed division is illustrated in Figure 5. For each region, the respective mean diameters were computed and the values are presented in Table 2.

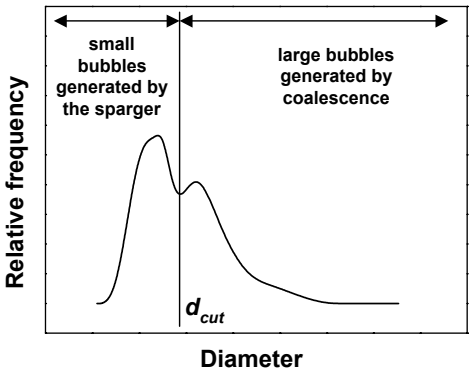

Figure 5: Schematic representation of the regions associated with the small and large bubbles.

Table 2: Mean diameters (experiments in duplicate) calculated for the small (S.B.) and large bubbles (L.B.).

U_G (cm/s)	d_{cut} (mm)	d_{10} (mm)		d_{30} (mm)		d_{32} (mm)	
		S.B.	L.B.	S.B.	L.B.	S.B.	L.B.
2.2	—	4.5 ± 0.1	—	4.9 ± 0.1	—	5.3 ± 0.8	—
		4.4 ± 0.1		4.7 ± 0.1		5.1 ± 0.7	
4.4	8.00	5.0 ± 0.1	9.5 ± 0.3	5.3 ± 0.1	9.8 ± 0.3	5.7 ± 0.8	10 ± 1
		4.8 ± 0.1	10.2 ± 0.3	5.2 ± 0.2	10.7 ± 0.3	5.6 ± 0.8	11 ± 2
6.6	10.0	5.9 ± 0.2	12.9 ± 0.4	6.4 ± 0.2	13.9 ± 0.4	7 ± 1	15 ± 2
		5.4 ± 0.2	13.1 ± 0.4	6.0 ± 0.2	13.9 ± 0.4	7 ± 1	15 ± 2
12.1	10.0	6.5 ± 0.2	13.4 ± 0.4	7.0 ± 0.2	14.1 ± 0.4	7 ± 1	15 ± 2
		6.5 ± 0.2	14.2 ± 0.4	7.0 ± 0.2	15.5 ± 0.4	7 ± 1	17 ± 2

With regard to the lowest gas superficial velocity, as the size distribution is unimodal, there are no large bubbles. For the other cases, though, it is important to highlight the significant difference between the values related to the two kinds of bubbles. With this division, the range of values for the three mean bubble diameters intercept, suggesting that even d_{10} provides a reasonable representation of the bubble size in each class, which did not occur when a single value for the whole distribution was estimated.

According to the reasoning applied in the division of the size distributions, the small bubbles would be the ones generated by the sparger and, consequently, their mean diameter may be estimated using thermofluid dynamic models, such as the one proposed by Campos and Lage (2000) for the

formation step. A comparison between the diameters predicted with that model and the experimental values is shown in Table 3. This table also includes the mean diameters determined for the whole distribution, without the division into classes. For isothermal processes, the comparison is usually made in terms of d_{30}, since bubble formation models actually calculate the bubble volume at the moment of detachment. However, in non-isothermal bubbling, the area of the bubble also becomes relevant on account of its influence upon heat and mass-transfer processes. As a result, the comparison was made in terms of both d_{30} and d_{32}.

For the lowest gas flow rate, the prediction errors, though greater than the experimental error, have the same order of magnitude as the ones reported by Polli et al. (2002). As for the other flow rates, when no division into classes is performed, both experimental mean bubble diameters are much larger than the value given by the model for the formation step, with most of the differences between these quantities being greater than twice the corresponding experimental error, a fact that provides evidence of coalescence effects. On the other hand, when only the first portion of the bubble size distribution is considered, experimental mean diameters in better agreement with the results predicted by the model of Campos and Lage (2000) are obtained. In this case, for d_{32}, the discrepancies between calculated and experimental values are either smaller than or equal to the experimental error. For d_{30}, the predicted values are rather close to the experimental estimates for both $U_G = 4.4$ and 6.6 cm/s, but the quality of the prediction is somewhat inferior for the highest gas flow rate. These outcomes suggest that the division proposed for the bubble size distribution is consonant with the idealised representation of the heterogeneous bubbling regime.

Table 3: Comparison between the predictions of the model proposed by Campos and Lage (2000), d_{calc}, and the experimental mean diameters (in duplicate) determined for the whole distribution (d_{whole}) and for the region of small bubbles (d_{SB}).

U_G (cm/)	d_{calc} (mm)	d_{30}						d_{32}					
		Experimental (mm)		Experimental error (%)		$100(d_{30} - d_{calc})/d_{30}$		Experimental (mm)		Experimental error (%)		$100(d_{32} - d_{calc})/d_{32}$	
		d_{whole}	d_{SB}	d_{whole}	d_{SB}	d_{whole}	d_{SB}	d_{whole}	d_{SB}	d_{whole}	d_{SB}	d_{whole}	d_{SB}
2.2	4.1	4.9	-	2.9	-	16	-	5.3	-	15	—	23	—
		4.7		2.5		13		5.1		14		20	
4.4	5.3	6.4	5.3	2.6	2.6	17	0	7	5.7	14	14	24	7.0
		6.4	5.2	3.0	3.1	17	-1.9	8	5.6	13	14	34	5.4
6.6	6.2	7.9	6.4	2.9	3.0	22	3.1	10	7	10	14	38	11
		8.3	6.0	3.1	2.8	25	-3.3	11	7	18	14	44	11
12.1	8.0	9.5	7.0	2.8	2.9	16	-14	11	7	18	14	27	-14
		10.7	7.0	2.8	3.0	25	-14	13	7	15	14	38	-14

Effect of the Sparger

As previously explained, apart from the stainless steel perforated plate, two other spargers were considered, namely a copper perforated plate and a stainless steel porous plate. In both cases, the runs were carried out for the three lower gas flow rates studied. Since changing the sparger in the experimental set-up was somewhat laborious, randomisation of the order of the runs was restricted to the operating gas flow rate for a given sparger. The bubble size distributions measured for each condition are portrayed in Figure 6. The different construction materials for the perforated plate distributor were actually tested on account of heat-transfer considerations, which are not dealt with in the present discussion.

In the case of the lowest gas superficial velocity, the two perforated plates, whose orifices have the same diameter, have quite similar bubble size distributions. The distribution for the porous plate is narrower, with the peak shifted to the left in comparison with those peaks observed for the perforated plates. This means a higher concentration of small bubbles, which is caused by the smaller orifice of the sparger. Consequently, the mean bubble diameter for the porous sparger is smaller, as shown in Table 4.

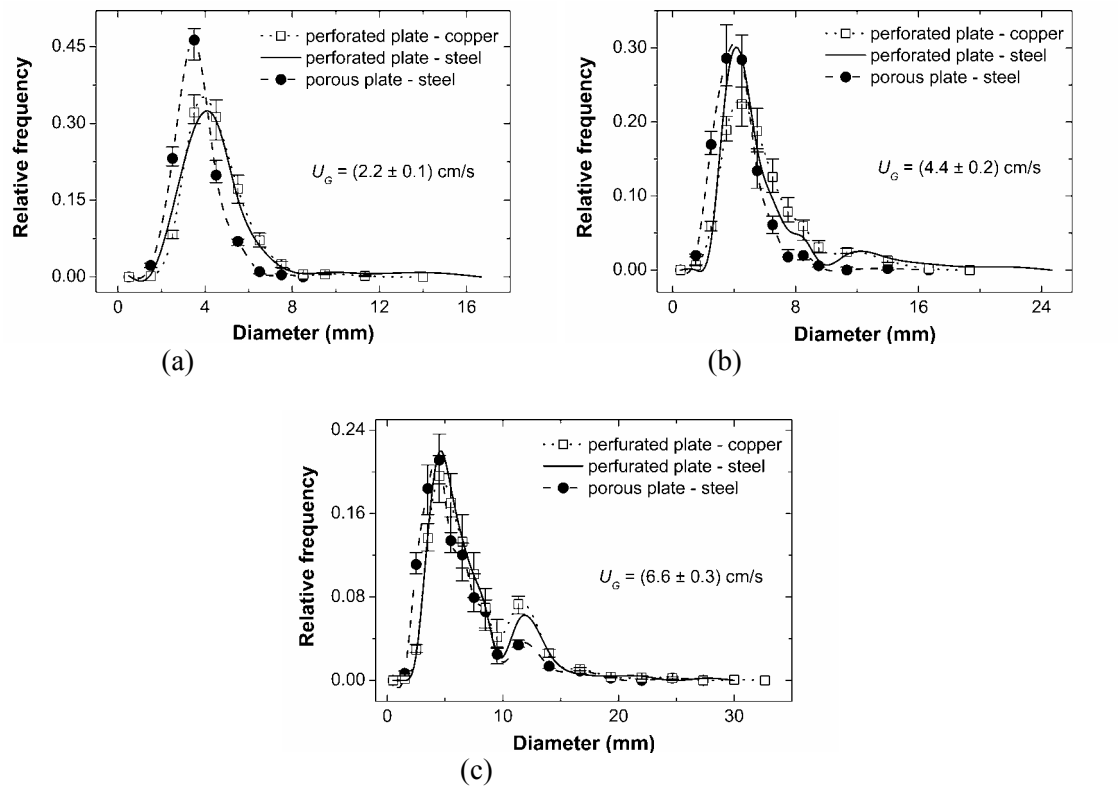

Figure 6: Bubble size distributions for the three spargers considered in this work.

Table 4: Mean bubble diameters for the three spargers and gas superficial velocities studied.

U_G (cm/s)	copper perforated plate	stainless steel perforated plate	stainless steel porous plate
d_{10} (mm)			
2.2	4.4 ± 0.1	4.5 ± 0.1 4.4 ± 0.1	3.6 ± 0.1
4.4	5.4 ± 0.2	5.7 ± 0.2 5.4 ± 0.2	4.3 ± 0.1
6.6	6.4 ± 0.2	6.6 ± 0.2 6.5 ± 0.2	5.6 ± 0.2
d_{30} (mm)			
2.2	5.1 ± 0.1	4.9 ± 0.1 4.7 ± 0.1	3.8 ± 0.1
4.4	6.9 ± 0.2	6.4 ± 0.2 6.4 ± 0.2	4.8 ± 0.2
6.6	7.9 ± 0.2	7.9 ± 0.2 8.3 ± 0.3	7.0 ± 0.2
d_{32} (mm)			
2.2	5.9 ± 0.8	5.3 ± 0.8 5.1 ± 0.7	4.1 ± 0.5
4.4	9 ± 1	7 ± 1 8 ± 1	5.3 ± 0.8
6.6	10 ± 1	10 ± 1 11 ± 2	9 ± 1

This effect of orifice diameter becomes less significant with the increase in gas superficial velocity due to intensification of the breakage and coalescence phenomena, which during the ascension step progressively alter the size distribution originally generated by the sparger. For U_G = 4.4 cm/s, the differences between the distributions associated with the stainless steel perforated and porous plates are much less pronounced than in the case of U_G = 2.2 cm/s. The data in Table 4 reveal that the mean bubble diameter is always smaller for the porous plate. Nonetheless, the difference between the mean diameters for the two lower gas superficial velocities is of about 25-40%, but it is reduced to approximately 15% when U_G = 6.6 cm/s. For the highest superficial velocity, the frequency of the breakage and coalescence phenomena is such that, even for a distance of about 0.11 m above the sparger, used for taking the photographs, the differences between the bubbles generated by the spargers had almost been eliminated. In this case, the d_{32} ranges have common values for the three spargers considered.

An interesting aspect of Figure 6 to which attention should be drawn is the fact that the distributions related to the two perforated plates for U_G = 4.4 cm/s do not bear as strong a resemblance to each other as the ones related to the lowest gas flow rate. Even though the error bars for the relative frequency intersect for most of the classes, the distribution associated with the copper plate seems to include a higher fraction of large bubbles, a hypothesis which is reinforced by the absence of common values in the computed ranges for d_{30}. The nominal value of d_{32} for the cupper plate is about 19% greater than the one for the stainless steel plate, but as the error associated with this diameter is considerable, the two ranges end up intersecting. For the copper plate, after the run with U_G = 4.4 cm/s, which was the last to be performed, many orifices in the plate were observed to be partially or even completely obstructed with a black material, probably composed of oxidation products. It is believed that the non-uniform gas distribution caused by the presence of these obstructions had contributed to the formation of larger bubbles on the sparger and to an increase in the coalescence rate in comparison with the stainless steel plate, which would explain the greater discrepancy observed between the perforated plates for U_G = 4.4 cm/s.

Effect of the Presence of Solutes

In the case of isothermal bubbling, data in the literature indicate that the addition of solutes to the continuous phase, either organic (Zieminski and Hill, 1962; Zieminski et al., 1967) or inorganic (Marrucci and Nicodemo, 1967; Lessard and Zieminski, 1971; Zahradník et al., 1995), prevents the bubbles from coalescing during the ascension step, and thus their size once again becomes a function of the sparger design. In order to verify whether or not this effect is to be expected in direct-contact evaporators, experiments with an aqueous 11.2 wt% sucrose solution were conducted.

When the porous plate was used as sparger, even for the lowest gas superficial velocity, the initially transparent sucrose solution became opaque and whitish as soon as bubbling commenced, so measurement of bubble size using the photographic technique was impossible with our equipment. However, the observed bubbles were visually smaller than those verified in distilled water.

For the stainless steel perforated plate, as the solution did not become opaque, quantitative analysis of the photographs could be carried out. In Figure 7 a comparison of the bubble size distributions in water and in the sucrose solution for U_G = 4.4 cm/s is presented. With the addition of sucrose, the range of variation in bubble size became smaller, as no bubbles with an equivalent diameter greater than 10 mm were observed. Moreover, there was a considerable increase in the relative frequency for bubbles whose equivalent diameters were between 2 and 4 mm. Additionally, the size distribution acquired the log-normal shape characteristic of the homogeneous bubbling regime (Akita and Yoshida, 1974; Parthasarathy and Ahmed, 1996; Lage and Espósito, 1999).

The mean bubble diameters quantified for these two systems using the bubble size distribution data are listed in Table 5. As none of the value ranges for the three mean diameters intersect, the smaller bubble size in the sucrose solution is further proved. For isothermal bubbling, a reduction in mean bubble diameter owing to the addition of sucrose to water was reported by Keitel and Onken (1982). Consequently, one concludes that this solute brings about coalescence hindrance in both isothermal and non-isothermal bubbling.

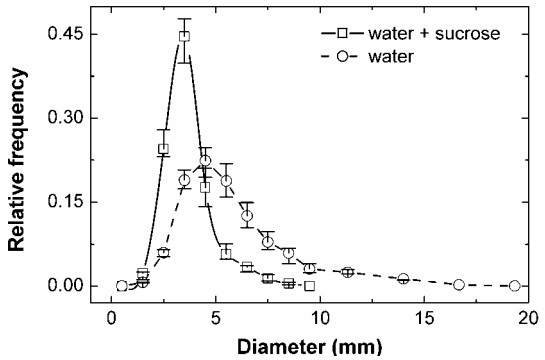

Figure 7: Comparison of the bubble size distributions in water and in the sucrose solution.

Table 5: Mean bubble diameters in water and in the 11.2 wt% sucrose solution.

Liquid	d_{10} (mm)	d_{30} (mm)	d_{32} (mm)
distilled water	5.7 ± 0.2	6.4 ± 0.2	7 ± 1
	5.4 ± 0.2	6.4 ± 0.2	8 ± 1
sucrose solution	3.7 ± 0.1	4.0 ± 0.1	4.4 ± 0.7

CONCLUSIONS

Using a photographic methodology, bubble size distributions in a direct-contact evaporator were experimentally determined under different operating conditions. For the three spargers tested, the size distribution, initially unimodal, became progressively bimodal as the gas superficial velocity, and consequently the breakage and coalescence frequencies, increased.

When the equipment operated in the homogeneous bubbling regime, the sparger with a smaller orifice gave smaller bubbles, but, in the coalescing system studied, the increase in gas superficial velocity eliminated the differences between the spargers. Similarly to what is observed for isothermal bubbling, the addition of solutes to the continuous phase led to coalescence hindrance.

ACKNOWLEDGEMENTS

The authors would like to thank CNPq (grant no. 520660/98-6) and FAPERJ (E-26/170.420/99-APQ1) for the financial support provided.

NOMENCLATURE

d	equivalent diameter of the bubble, m
d_{cut}	diameter that defines the limits between the two bubbles classes in the division of the bubble size distribution, m
d_{pq}	mean bubble diameter defined by Eq. (3), m
d_{SB}	mean diameter for the small bubbles region of the size distribution, m
d_{whole}	mean diameter for the whole bubble size distribution, m
F	normalised density function of the bubble size distribution, -
H_i	relative frequency of bubbles in class i,
h_i	lower limit for class i, m
h_{i+1}	upper limit for class i, m
NB	total number of bubbles analysed for a given experimental condition, -
NC	total number of classes, -
U_G	gas superficial velocity, m/s
δ	delta function, -
ΔH_i^+	positive deviation of the relative frequency for class i, -
ΔH_i^-	negative deviation of the relative frequency for class i, -

REFERENCES

Akita, K. and Yoshida, F., Bubble Size, Interfacial Area and Liquid-phase Mass transfer Coefficient in Bubble Columns, Industrial and Engineering

Chemistry, Process Design and Development, 13, No. 1, 84 (1974).

Camarasa, E., Vial, C., Poncin, S., Wild, G., Midoux, N. and Bouillard, J., Influence of Coalescence Behaviour of the Liquid and of Gas Sparging on Hydrodynamics and Bubble Characteristics in a Bubble Column, Chemical Engineering and Processing, 38, 329 (1999).

Campos, F.B. and Lage, P.L.C., Heat and Mass Transfer Modelling During the Formation and Ascension of Superheated Bubbles, International Journal of Heat and Mass Transfer, 43, No. 16, 2883 (2000).

Colella, D., Vinci, D., Bagatin, R., Masi, M. and Bakr, E.A., A Study on Coalescence and Breakage Mechanisms in Three Different Bubble Columns, Chemical Engineering Science, 54**,** No. 21, 4767 (1999).

Cronan, C.S., Submerged Combustion Flares Anew, Chemical Engineering, 63, No. 2, 163 (1956).

Ellenberger, J. and Krishna, R., A Unified Approach to the Scale-up of Gas-Solid Fluidised Bed and Gas-Liquid Bubble Column Reactors, Chemical Engineering Science, 49, No. 24B, 5391 (1994).

Hebrard, G., Bastoul, D. and Roustan, M., Influence of the Gas Sparger on the Hydrodynamic Behaviour of Bubble Columns, Chemical Engineering Research and Design, 74, No. A3, 406 (1996).

Keitel, G. and Onken, U., Inhibition of Bubble Coalescence by Solutes in Air/Water Dispersions, Chemical Engineering Science, 37, No. 11, 1635 (1982).

Kölbel, H., Borchers, E. and Langemann, H., Bubble Size Distribution in Bubble Columns: Influence of Liquid Viscosity and Column Pressure, Chemie Ingenieur Technik, 33, No. 10, 668 (1961) (in German).

Lage, P.L.C. and Espósito, R.O., Experimental Determination of Bubble Size Distributions in Bubble Columns: Prediction of Mean Bubble Diameter and Gas Hold-up, Powder Technology, 101, No. 2, 142 (1999).

Lessard, R.R. and Zieminski, S.A., Bubble Coalescence and Gas Transfer in Aqueous Electrolytic Solutions, Industrial and Engineering Chemistry Fundamentals, 10, No. 2, 260 (1971).

Marrucci, G. and Nicodemo, L., Coalescence of Gas Bubbles in Aqueous Solutions of Inorganic Electrolytes, Chemical Engineering Science, 22, No. 9, 1257 (1967).

Mezavilla, A.C., Direct-contact Evaporation: Heat and Mass Transfer During the Formation of Superheated Bubbles, Master's thesis, Federal University of Rio de Janeiro (1995) (in Portuguese).

Millies, M. and Mewes, D., Interfacial Area Density in Bubbly Flow, Chemical Engineering and Processing, 38, 307 (1999).

Nelson, T.J., Tnimage Scientific Image Analysis Software Transforming and Numeric Image Analysis System, ftp://sunsite.unc.edu/pub/linux/apps/graphics/misc/ (Linux version) (2000).

Parthasarathy, R. and Ahmed, N., Size Distribution of Bubbles Generated by Fine-pore Spargers, Journal of Chemical Engineering of Japan, 29, No. 6, 1030 (1996).

Polli, M., Stanislao, M., Bagatin, R., Bakr, E.A. and Masi, M., Bubble Size Distribution in the Sparger Region of Bubble Columns, Chemical Engineering Science, 57, No. 1, 197 (2002).

Prince, M. J. and Blanch, H. W., Bubble Coalescence and Break-up in Air-sparged Bubble Columns, AIChE Journal, 36, No. 10, 1485 (1990).

Ruzicka, M.C., Zahradnik, J., Drahos, J. and Thomas, N.H., Homogeneous-heterogeneous Regime Transition in Bubble Columns, Chemical Engineering Science, 56, 4609 (2001).

Schäfer, R., Merten, C. and Eigenberger, G., Bubble Size Distributions in a Bubble Column Reactor under Industrial Conditions, Experimental Thermal and Fluid Science, 26, No. 6-7, 595 (2002).

Silva, L.F.L.R. and Lage, P.L.C., Gas Hold-up and Bubble Sizes in Non-isothermal Bubble Columns, Proceedings of the XXVIII Brazilian Congress on Particulate Systems, 207 (2000) (in Portuguese).

Todtenhaupt, E.K., Bubble Size Distribution in Technical Gas Dispersed Devices, Chemie Ingenieur Technik, 43, No. 6, 336 (1971) (in German).

Vermeer, D. J. and Krishna, R., Hydrodynamics and Mass Transfer in Bubble Columns Operating in the Churn-turbulent Regime, Industrial and Engineering Chemistry, Process Design and Development, 20, 475 (1981).

Zahradník, J., Fialová, M., Kastanek, F., Green, K.D. and Thomas, N.H., The Effect of Electrolytes on Bubble Coalescence and Gas Hold-up in Bubble Column Reactors, Chemical Engineering Research and Design, 73, No. A3, 341 (1995).

Zieminski, S.A. and Hill, R.L., Bubble Aeration of Water in the Presence of Some Organic Compounds, Journal of Chemical and Engineering Data, 7, No. 1, 51 (1962).

Zieminski, S.A., Caron, M.M. and Blackmore, R.B., Behavior of Air Bubbles in Dilute Aqueous Solutions, Industrial and Engineering Chemistry Fundamentals, 6, No. 2, 233 (1967).

APPENDIX

Let F(d) be the normalised density function for a bubble population. Given two diameters, h_i and h_{i+1} ($h_i < h_{i+1}$), the fraction of bubbles H_i whose diameters fall between the two specified values is given by:

$$H_i = \int_{h_i}^{h_{i+1}} F(d)\ d(d) \tag{A.1}$$

Experimentally, this quantity is estimated as the relative frequency of class i for a finite set of NB bubbles. Using the step function, u(x), defined by the relation

$$u(x) = \begin{cases} 0 & \text{for } x < 0 \\ 1 & \text{for } x \geq 0 \end{cases} \tag{A.2}$$

the number of bubbles N_i whose diameters lie between h_i and h_{i+1} can be expressed by the following equation:

$$N_i = \sum_{j=1}^{NB} \left[u(d_j - h_i) - u(d_j - h_{i+1}) \right] \tag{A.3}$$

so the experimental value of H_i (relative frequency) is given by

$$H_i = \frac{N_i}{NB} = \frac{\sum_{j=1}^{NB} \left[u(d_j - h_i) - u(d_j - h_{i+1}) \right]}{NB} \tag{A.4}$$

The partial derivative of H_i in relation to a diameter, d_k, of one of the NB bubbles from the data set is:

$$\frac{\partial H_i}{\partial d_k} = \frac{1}{NB} \sum_{j=1}^{NB} \left[\frac{d\,u(d_j - h_i)}{d(d_k)} - \frac{d\,u(d_j - h_{i+1})}{d(d_k)} \right] \tag{A.5}$$

Since the derivative of the step function is the delta function, δ, and the summation terms in Eq. (A.5) will only not be zero when j = k, the previous equation is rewritten as

$$\frac{\partial H_i}{\partial d_k} = \frac{1}{NB} \left[\delta(d_k - h_i) - \delta(d_k - h_{i+1}) \right] \tag{A.6}$$

Utilising Eq. (A.6), the total differential of H_i becomes

$$dH_i = \sum_{k=1}^{NB} \left(\frac{\partial H_i}{\partial d_k} \right) d(d_k) = \frac{1}{NB} \sum_{k=1}^{NB} \left[\delta(d_k - h_i) - \delta(d_k - h_{i+1}) \right] \tag{A.7}$$

Provided that the integration limits are properly chosen, Eq. (A.7) can be used for estimating the positive and negative deviations of H_i. Starting with the positive deviation, the experimental errors in d_k can increase the value of H_i, either with a positive deviation for a diameter smaller than h_i or with a negative deviation for a diameter larger than h_{i+1}. Thinking in terms of a maximum error, these two contributions are added, thereby obtaining Eq. (1). For the negative deviation, the contributions of the experimental errors, Δd_k, are opposite to those verified for the positive deviation, so a similar reasoning results in Eq. (2).